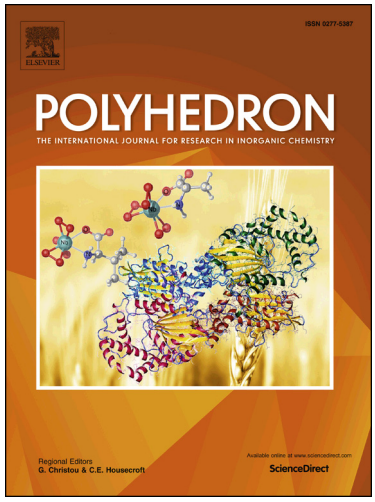

A novel oxidovanadium(V) compound with an isonicotinohydrazide ligand. A combined experimental and theoretical study and cytotoxity against K562 cells.

Ana C. González-Baró, Verónica Ferraresi-Curotto, Reinaldo Pis-Diez, Beatriz S. Parajón Costa, Jackson A.L.C. Resende, Flávia C.S. de Paula, Elene C. Pereira-Maia, Nicolás A. Rey

PII: S0277-5387(17)30496-5
DOI: http://dx.doi.org/10.1016/j.poly.2017.07.013
Reference: POLY 12749

To appear in: *Polyhedron*

Received Date: 29 May 2017
Revised Date: 18 July 2017
Accepted Date: 20 July 2017

Please cite this article as: A.C. González-Baró, V. Ferraresi-Curotto, R. Pis-Diez, S.P. Costa, J.A.L. Resende, F.C.S. de Paula, E.C. Pereira-Maia, N.A. Rey, A novel oxidovanadium(V) compound with an isonicotinohydrazide ligand. A combined experimental and theoretical study and cytotoxity against K562 cells., *Polyhedron* (2017), doi: http://dx.doi.org/10.1016/j.poly.2017.07.013

A novel oxidovanadium(V) compound with an isonicotinohydrazide ligand. A combined experimental and theoretical study and cytotoxity against K562 cells.

Ana C. González-Baró[a*], Verónica Ferraresi-Curotto[a(1)], Reinaldo Pis-Diez[a], Beatriz S. Parajón Costa[a], Jackson A. L. C. Resende[b], Flávia C. S. de Paula[c], Elene C. Pereira-Maia[c], Nicolás A. Rey[d]

[a]CEQUINOR (CONICET-CCT-La Plata, UNLP), Bvd 120 N1465 1900 La Plata, Argentina.

[b] Instituto de Ciências Exatas e da Terra, CUA/UFMT, Barra do Garças, MT, Brazil.

[c] Departamento de Química, UFMG, Belo Horizonte, MG, Brazil.

[d] LABSO-BIO, Departamento de Química, PUC-Rio, Rio de Janeiro, RJ, Brazil.

[(1)] Current affiliation IFLP (CONICET, UNLP), CC 67, B1900AVV La Plata, Argentina.

* e-mail: agb@quimica.unlp.edu.ar

Abstract

The interaction of oxidovanadium(V) with INHOVA (the condensation product of isoniazid and *o*-vanillin) lead to the formation of the ester-like complex [VO(INHOVA) $EtO(OH_2)$]$Cl{\cdot}H_2O$ (**1**). Crystals suitable for X-ray diffraction methods were obtained. The complex crystallizes as a dimer in the space group $P2_1/c$ of the monoclinic system. A detailed analysis, including solid-state vibrational spectroscopy and electronic spectroscopy in DMSO solution, was performed for both INHOVA and complex (**1**). A complete theoretical study based on DFT was also carried out. The calculations were of valuable assistance in the spectra assignments and interpretation. The electrochemical characterization allows determining the redox behavior of INHOVA and complex (**1**). Cytotoxicity was assayed against the *chronic myelogenous leukemia* K562 cell line. The IC_{50} values obtained denote that both the ligand and complex (**1**) are good candidates for further studies.

Keywords: oxidovanadium(V), isoniazid, *o*-vanillin, structural study, DFT calculations, cytotoxicity.

1. Introduction

Condensation reaction of the antituberculosis agent isoniazid (isonicotinic acid hydrazide, INH) [1] with *o*-vanillin (2-hydroxy-3-meyhoxybenzaldehyde, *o*-HVa) leads to the formation of a stable and active hydrazone, N'-[(1E)-(2-hydroxy-3-methoxyphenyl)methylene]isonicotinohydrazide, INHOVA (see Scheme 1). It is an interesting member of the family of Schiff bases containing aromatic rings with a OH group in *ortho* position to the imino moiety. This kind of compounds are of relevance mainly due to the existence of either O–H···N or O···H–N hydrogen bonds and the tautomerism between enol-imine and keto-amine forms. Moreover, some hydrazones of INH with hydroxyaldehydes have shown conserved activity and less toxicity upon inactivation of the NH_2 group of the parent hydrazide [2]. In particular, a group of hydrazones were found to be even more effective than INH itself as antituberculosis agents [3,4].

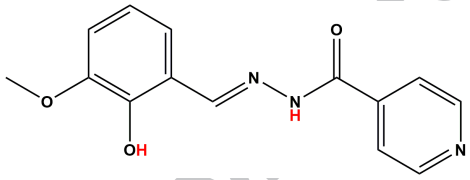

Scheme 1. INHOVA

INHOVA has been previously obtained and its crystal structure has been determined [5-7]. Moreover, a detailed structural, spectroscopic and theoretical study has been reported by our group [8].

In the field of coordination chemistry, this type of hydrazones has received special attention as polyfunctional ligands in metal complexes, including vanadium centers [9,10]. This kind of hydrazones and their metal complexes exhibit a variety of biological and pharmaceutical activities, being recognized as antimicrobial, antituberculosis, antitumoral and antioxidant agents [11-13]. Cytotoxicity assays of some organotin(IV) complexes containing INHOVA in a series of human cancer cell lines placed them as promising anticancer agents [14].

In addition to the widely known therapeutic properties of oxidovanadium(V) compounds, such as their insulin-mimetic activity, there is a growing interest in vanadium compounds as potential therapeutic agents for the treatment of cancer [15-17]. A complex of this metal with an *o*-HVa-derived Schiff base ligand has been determined to bind to CT-DNA in a non-classical intercalative mode and to possess a strong affinity with the BSA protein, inducing

conformational changes [18]. Among the immense variety of oxidovanadium(V) complexes, some examples of ester-like coordination compounds containing organic ligands, including hydrazones, have been reported [19-23]. The structure of a complex containing this metal as the VO_2 center coordinated to a ligand closely related to INHOVA has been described but only briefly discussed [24].

In this work, the interaction of oxidovanadium(V) with INHOVA was studied in an attempt to obtain metal complexes of therapeutic interest. The complex [VO(INHOVA) EtO(OH_2)]Cl·H_2O (**1**, Scheme 2) was prepared from ethanolic solutions of the reactants and obtained as crystals suitable for X-ray structure determination. As a consequence of the protonation of the pyridinic nitrogen, the INHOVA ligand appears as a monoanion. An extensive characterization, including vibrational spectroscopy of the solid, and electronic spectroscopy and electrochemical analysis in solution, was performed. A complete theoretical study based on DFT was also carried out. The calculations were of valuable assistance in the spectra assignments and interpretation. Cytotoxicity on K562 cells was evaluated for both INHOVA and complex (**1**), with promising results.

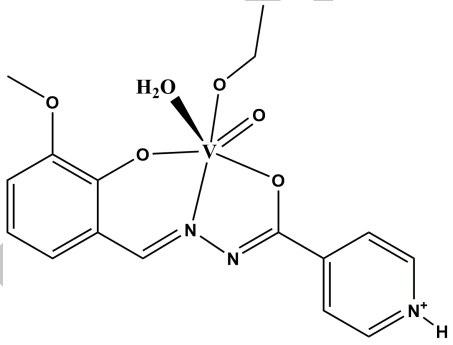

Scheme 2. The complex cation [VO(INHOVA) EtO(OH_2)]$^+$

2. Experimental

2.1. Syntheses

INH and *o*-HVA were acquired from Sigma-Aldrich, HCl and $VOCl_2$ (50% aqueous hydrochloric solution) from Carlo Erba and EtOH from Biopack, all of them of analytical grade, were used as purchased.

2.1.1 Synthesis of the ligand.

The hydrazone was prepared according to the procedure previously reported [8]. Even when it was obtained as a chloride of the pyridinium salt ($INHOVAH^+Cl^-$), it will be referred as INHOVA, as it has been named in previous publications.

2.1.2. Synthesis of the complex (**1**).

0.2 mmol of INHOVA (0,0633 g) were dissolved in 30 mL of EtOH under heating and stirring. The resulting solution was dropwise added to a mixture of 0.2 mmol of $VOCl_2$ (110 μL) with 10 mL of EtOH, while stirring, leading to an amber-colored solution. The system was then refluxed during 3 hours turning to a darker colour. After standing at room temperature for a couple of weeks, a crystalline solid was observed. The caramel-colored crystals were filtered off, washed with cold EtOH and dried in a desiccator.

2.2- X-ray diffraction data

Single crystal X-ray diffraction experiment was performed in a Bruker-Nonius Kappa-CCD diffractometer at room temperature using MoKα radiation. The structure was solved by direct methods using SHELXS and refined by full-matrix least-squares on F^2 using SHELXL-97. All non-hydrogen atoms were refined using anisotropic displacement parameters. The hydrogen atoms were generated in idealized geometries, and they were refined according to the riding model. The carbon atoms C12e and C22e, belonging to the ethoxo ligand, were described disordered with occupation of 39% and 61%, respectively.

2.3- Spectroscopic analysis

The FTIR spectra were obtained with a Bruker EQUINOX 55 spectrometer in KBr discs with 4 cm^{-1} resolution and 60 scans, in the 4000-400 cm^{-1} range. The electronic absorption spectra were measured in DMSO and EtOH (1×10^{-5} M) in the 200-800 nm spectral range. They were recorded with a Hewlett-Packard 8452-A diode array spectrometer using 10 mm quartz cells.

2.4. Computational methods

The X-ray structure of the complex cation present in (**1**) was taken as the starting geometry for optimization. The geometry optimization was conducted in vacuum and was performed with the GGA B97-D exchange-correlation functional that includes long-range

dispersion corrections [25]. The 6-311G(d,p) basis set was used for H, C, N and O, whereas the LANL2TZ pseudopotential was employed for V. After optimization, the Hessian matrix of the total electronic energy with respect to the nuclear coordinates was constructed and diagonalized to check whether the optimized structure is a local minimum on the potential energy surface of the complex. The eigenvalues of the hessian matrix were then converted to harmonic vibrational frequencies that can be compared with experimental frequencies.

Vertical electronic transitions were calculated with the one-parameter hybrid GGA PBE0 exchange-correlation functional [26] using the geometry optimized with the B97-D functional. In this case, diffuse functions were added to the 6-311G(d,p) basis set for N and O. The IEF-PCM method [27] was used to include implicitly solvent effects (DMSO and EtOH) in the calculation of the electronic transitions. All the calculations were performed with the Gaussian 09 program [28].

2.5. Electrochemical characterization

The redox behavior of INHOVA and complex (1) was determined by cyclic voltammetry in DMSO and EtOH solutions using a computer controlled potenciostat/galvanostat PAR model 263A. Tetrabutylammonium hexafluorophosphate ($TBAPF_6$) was employed as supporting electrolyte (Fluka , electrochemical grade).

Measurements were performed on a glassy carbon disc electrode in absence of O_2 at different scan rates (v). A continuous gas stream was passed over the solution during the measurements A platinum wire was used as counter electrode, whereas Ag/(10^{-3}M) $AgNO_3$, in CH_3CN /10^{-1} M $(TBA)PF_6$, was employed as reference electrode. This electrode was calibrated against the $[Fe(C_5H_5)_2]/[Fe(C_5H_5)_2]^+$ redox couple, for which a potential of +0.17V was determined.

2.6. Cytotoxicity assays

The ligand and the metal complex were tested against the *chronic myelogenous leukemia* K562 cell line, purchased from the Rio de Janeiro Cell Bank (number CR083 of the RJCB collection). It was established from the pleural effusion of a 53 year old female with chronic myelogenous leukemia in terminal blast crisis. Cells were cultured in RPMI 1640 medium supplemented with 10% fetal calf serum (CULTLAB, São Paulo, Brazil) at 37 ℃ in a humidified 5% CO_2 atmosphere. Cultures grow exponentially from 10^5 cells mL^{-1} to about

10^6 cells mL^{-1} in 3 days. Cell viability was checked by Trypan Blue exclusion. Cell number was determined by Coulter counter analysis.

For cytotoxicity assessment, 1×10^5 cell mL^{-1} were cultured for 72 h in the absence and the presence of various concentrations of the compounds. The sensitivity to INHOVA and its oxidovanadium(V) complex was evaluated by the concentration needed to inhibit cell growth by 50%, the IC_{50}. Stock solutions of the compounds were prepared in DMSO. The final concentration of DMSO in the experiments with cells was below 0.5% and we have checked that the solvent has no effect on cell growth at this concentration.

3. Results and discussion

3.1. Crystal Structure

The solid crystalized as a chloride salt of the cationic complex, in the monoclinic system, space group $P2_1/c$. Crystal data and structure refinement results are summarized in Table 1. The ligand acts in a tridentate manner through the O,N,O-donor system constituted by the deprotonated phenol O4, the N1 atom of the hydrazonic linkage and the enolate oxygen O3. It appears as a monoanion ($INHOVA^-$) as a consequence of the protonation of the pyridinic nitrogen. The distorted octahedral coordination environment is completed by an oxo ligand, a disordered solvent-derived ethoxide anion and a water molecule. An ORTEP drawing is shown in Figure 1.

The crystalline packing (Figure 2) shows that complex cations aggregate into a dimer [R^2_2 (10)] by means of moderate intermolecular H-bonds involving the coordinated water molecule and the nitrogen atom N2 [O1W···N2 =2.907(3) Å]. The interaction of complex cations with chloride counter-ions and crystallization water molecules stabilizes the bilayer overall arrangement along the (-100) plane. Corresponding intra-molecular bond distances and angles can be obtained directly from the available *.cif* file.

Table 1. Crystal data and structure refinement results for complex (**1**).

Empirical formula	$C_{16}H_{21}N_3O_7VCl$
Formula weight	453.76
Temperature/K	293(2)
Crystal system	Monoclinic
Space group	$P2_1/c$
a/Å	8.7126(17)
b/Å	23.170(5)
c/Å	9.945(2)
α/°	90
β/°	100.97(3)
γ/°	90
Volume/Å^3	1970.8(7)
Z	4
ρ_{calc}g/cm^3	1.5292
μ/mm^{-1}	0.682
F(000)	938.3
Crystal size/mm^3	0.21 × 0.08 × 0.02
Radiation	Mo Kα (λ = 0.71073)
2Θ range for data collection/°	6.7 to 50.7
Index ranges	−10 ≤ h ≤ 11, −29 ≤ k ≤ 30, −12 ≤ l ≤ 12
Reflections collected	23755
Independent reflections	3579 [R_{int} = 0.0456, R_{sigma} = 0.0472]
Data/restraints/parameters	3579/6/256
Goodness-of-fit on F^2	1.069
Final R indexes [I>=2σ (I)]	R_1 = 0.0379, wR_2 = 0.0856
Final R indexes [all data]	R_1 = 0.0612, wR_2 = 0.0975
Largest diff. peak/hole / e Å^{-3}	0.37/−0.36

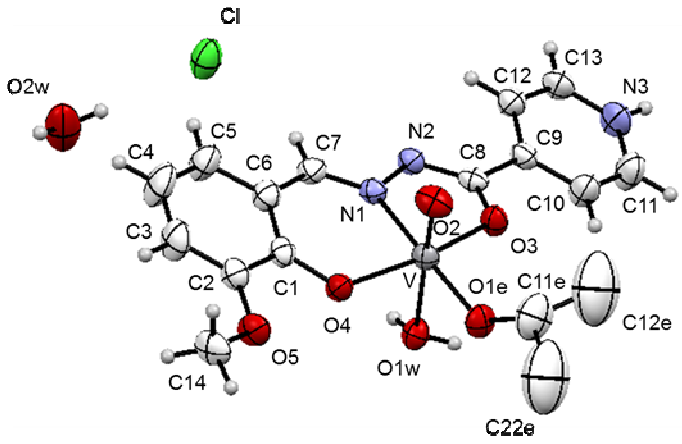

Figure 1. ORTEP representation (50% probability ellipsoids) of complex (**1**). H-atoms in the disordered ethoxide ligand are omitted for clarity.

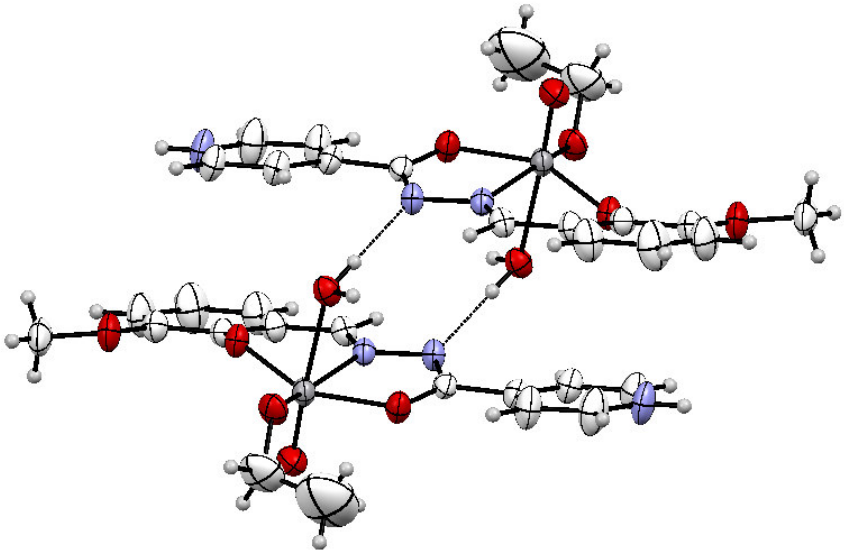

Figure 2. Dimer in the crystalline packing of complex (**1**) (disordered atoms, the crystallization water molecules and chloride counter-ions are omitted for the sake of clarity)

3.2. Geometry optimization and comparison with experimental results

Selected geometrical parameters obtained after geometry optimization are listed in Table 2. Experimental information is also shown in that table. The optimized parameters agree very well in general with experimental data. The V-O1w bond distance is predicted to be more than 0.3 Å larger than the experimental value, see Figure 1 for labels. It is argued that this is due to the fact that the water molecule is stabilized at a shorter V-O distance by intermolecular H-bonds as it is shown in Figure 2 for the packing in the solid state.

Intermolecular interactions are obviously absent in the calculation carried out for the isolated complex, thus water molecules bound to the V ion through H-bonds could be able to stabilize at larger distances. On the other hand, the other V-O bond distances show a very good agreement with experimental data, with an average error of only 0.013 Å. The V-N bond distance agrees also very well with the experimental value, being only 0.024 Å larger. Those findings reinforce the argument given above in the sense that the V-O and V-N bond distances are well reproduced when neither the O atoms or the N atoms are involved in intermolecular H-bonds. Maximum errors in bond angles are about 8 degrees and involve the oxygen atom of the water molecule, namely, α(O4-V-O1w), α(O2-V-O1w) and α(N1-V-O1w). Dihedral angles are very well described by the calculated parameters. The largest error is observed in τ(O4-V-O3-C), for which a deviation of 20 degrees from experimental values is found. The calculations seem to suggest that the environment of the V(V) ion is almost unaltered when the solid is formed, with the exception of the water molecule, which is further stabilized at a shorter distance of the metallic ion by neighbor molecules, thus completing its coordination sphere.

Table 2. Experimental and calculated geometric parameters. Distances (d) are in Å and bond and dihedral angles (α and τ, respectively) are in degrees. See Figure 1 for labels.

	Exp.	Calc.		Exp.	Calc.
d(V-O2)	1.577 (2)	1.591	α(O2-V-O1w)	177.32 (10)	170.1
d(V-O1e)	1.769 (2)	1.776	α(O1e-V-O1w)	79.34 (9)	83.1
d(V-O4)	1.859 (2)	1.883	α(O4-V-O1w)	82.17 (9)	73.0
d(V-O3)	1.984 (2)	1.992	α(O3-V-O1w)	79.59 (9)	77.2
d(V-N1)	2.116 (2)	2.140	α(N1-V-O1w)	84.20 (9)	76.3
d(V-O1w)	2.323 (2)	2.695	τ(O2-V-O4-C)	50.6 (3)	53.6
α(O2-V-O1e)	101.64 (12)	106.6	τ(O1e-V-O4-C)	155.5 (2)	164.0
α(O2-V-O4)	99.94 (11)	102.6	τ(O3-V-O4-C)	−78.2 (3)	−86.8
α(O1e-V-O4)	104.71 (10)	102.4	τ(N1-V-O4-C)	−42.7 (2)	−39.5
α(O2-V-O3)	97.84 (11)	104.0	τ(O1w-V-O4-C)	−127.7 (3)	−117.3
α(O1e-V-O3)	92.52 (9)	90.2	τ(O2-V-O4-C)	−93.6 (2)	-84.1
α(O4-V-O3)	152.06 (9)	145.8	τ(O1e-V-O3-C)	164.3 (2)	168.7
α(O3-V-N1)	94.36 (11)	94.5	τ(O4-V-O3-C)	35.6 (3)	56.0
α(O1e-V-N1)	160.37 (10)	156.2	τ(N1-V-O3-C)	−1.3 (2)	6.6
α(O4-V-N1)	83.36 (9)	83.1	τ(O1w-V-O3-C)	85.6 (2)	85.8
α(O3-V-N1)	73.92 (9)	73.8			

3.3. Infrared spectroscopy

The IR spectrum was analyzed in comparison with that corresponding to the free ligand (INHOVA). Experimental and calculated values of the selected spectral signals are depicted in Table 3, together with the respective assignments, done with the help of theoretical results. A complete list of frequencies and respective assignments are provided as Supplementary Material (Table S1). Figure 3 shows the registered spectra in the more relevant region.

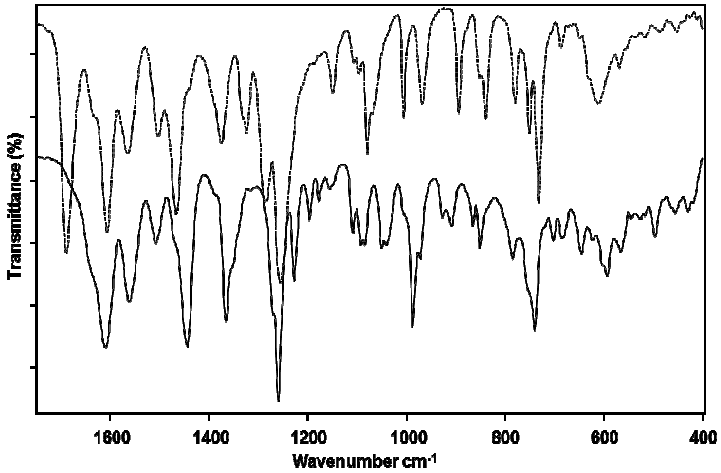

Figure 3. IR spectra in the 1800-400 cm^{-1} spectral region. Ligand (dotted line, top), and complex (solid line, bottom)

Table 3. Selected experimental and calculated IR data (4000-400 cm^{-1}) of complex (**1**) and INHOVA. Reported frequencies are in cm^{-1}.

INHOVA	Calc[(a)]	Complex (1)	Calc.	Assignment
		3366 s	3828	$\nu_{as}(H_2O)$coord.
		3272 s	3718	$\nu_{s}(H_2O)$coord.
3157 w	3492			νNH(hydrazone)
3014 w	3594			νOH
		2932 w	3058	$\nu_{as}CH_3$(ethoxo)
			3043	
		2905 sh	2956	$\nu_{s}CH_3$(ethoxo)
		2804 vw	2898	$\nu_{s}CH_2$(ethoxo)
2590m,b	3513	2650 w,b	3529	νN3H
1688 vs	1795			νC=O
1606 vs	1689			νC=N
			1611	$\delta(H_2O)$cord.
		1609 s	1565	νC=N1 + νC=N2
		1444 s	1450	νO3-C=N2 + δCH(INH)
1374 m	1338			δOH
		1365 s	1409	νC-O4(V) + ν(coord ring *o*-HVA) (see text)
			1379	ν(coord ring *o*-HVA) (see text)
		1270 m	1333	$\rho_{w}CH_2$

1256 vs	1263	1259 vs	1265	νAr-OCH_3 + δCH(*o*-HVA)
		1228 m	1234	νC-O4(V) + δCH(all) + δN3H
		987 s	1036	νV=O2 + ν_{as} (C-C-O1e)
893 m	612			γOH
		593 w	593	νN1-V
		566 w	565	νV-O4 + γring(*o*-HVA)
		496 w	556	νV-O3

(a) Data from ref. [8].

Calculations show a strong coupling of several modes. The assignments were done taking into account predominant vibrations at each frequency. Regarding the present results, the previously reported assignment of the ligand spectrum [8] has been revised. Some differences were found that can be attributed, at least in part, to the change in the functional employed in the DFT calculations, used to help in the assignments.

Characteristic stretching bands of coordinated water are present in the complex spectrum, whereas the one expected for the bending mode of this molecule (calculated value: 1611 cm^{-1}) should be overlapped with the strong band at 1609 cm^{-1}. This band is related to the out of phase C=N stretchings in the –C=N1-N2=C- moiety, characteristic of enolate coordination of hydrazones. in accordance with the crystallographic results.

The INHOVA spectrum shows a broad intense band at 2590 cm^{-1} assigned to the pyridinic N-H stretching according to the data reported for this mode in related compounds [29]. The complex spectrum shows a poorly resolved broad band centered at approximately 2650 cm^{-1} which can be attributed to this vibration. The discrepancies between experimental and calculated frequencies are expected since vibrations including atoms involved in H-bonds are always overestimated. In this case, N3-H interacts with one of the lone electron pairs of a crystallization water molecule.

The bands assigned to C-H stretching modes of the ethoxo group appear between 2932 and 2804 cm^{-1} in the spectrum of the complex.

Bands assigned to modes involving phenolic OH and hydrazone NH groups in the ligand are absent after coordination to the metal. Moreover, the strong band attributed to C=O3 stretching in INHOVA disappears in the spectrum of (1). Calculations indicate that the new band at 1444 cm^{-1} in the spectrum of (1) can be attributed to the stretching of O3-C=N2 linkage, involving the coordinated atoms of the INH fragment. Additionally, the band at 1365 cm^{-1} in the spectrum of the complex is assigned to the νC-O4(V) mode coupled with the stretchings involving C1-C6-C7-N1atoms of INHOVA (coordination ring *o*-HVA). These results are in accordance with the ONO donor system of the tridentate ligand.

Oxovanadium moiety (V=O2) stretching, coupled with asymmetric C-C-O1e mode, appears in the spectrum of the complex, as a typical band at 987 cm^{-1}. The bands assigned to the ethoxo group can be observed at expected frequencies and V-ligand modes are present in the predicted spectral region.

3.4. Electronic spectroscopy

The absorption spectra of the complex and the free ligand were recorded both in DMSO and in EtOH. Results indicate that no appreciable differences exist between the spectra of each compound in both solvents. Thus, only the spectra obtained in EtOH are presented, because the lower wavelength cut-off of that solvent allows the study of a wider spectral region. The spectra are shown in Figure 4, whereas experimental absorption maxima and calculated transition energies are listed in Table 4. Measurements in DMSO were useful to determine solutions stability, as the biological assays are carried out from stock solutions prepared in this solvent.

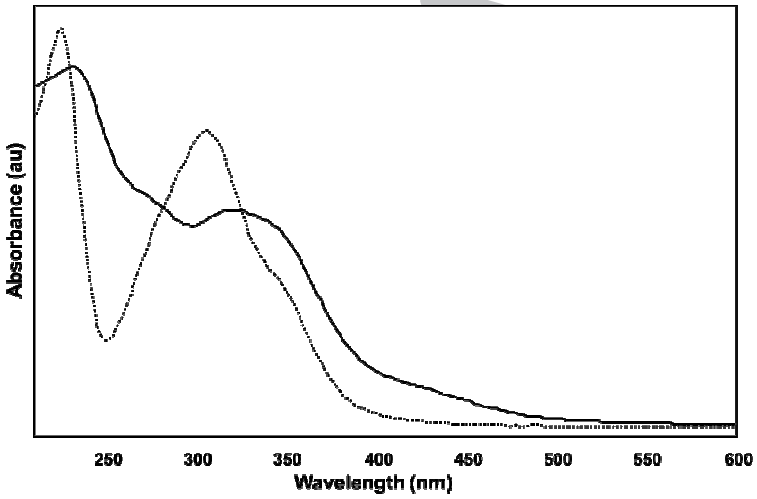

Figure 4. Electronic absorption spectra of complex (**1**) (solid line) and INHOVA (dotted line) in EtOH (1 x 10^{-5} M) in the 210-600 nm spectral range.

In all cases, experimental bands are described by at least two one-electron excitations indicating that the complex under study is dominated by many-body effects. For simplicity, only the dominant transitions are used to assign the experimental bands. Dominant transitions are chosen according to their oscillator strengths. Calculated transitions describe very well the experimental bands as can be deduced from Table 4.

Table 4. Experimental absorption bands and calculated electronic transitions, in nm, for [VO(INHOVA) EtO(OH_2)]$^+$ in EtOH solution. Oscillator strengths, in atomic units, are also given. The proposed assignment based on calculations is provided. Percent contribution of one-electron excitations to the transitions and their assignment in terms of chemical species is given in parentheses. Only those calculated electronic transitions relevant for the assignments are listed.

Exp.	Calc.	Osc. str.	Assignment
424	429	0.2333	HOMO – 1 → LUMO + 1 (44%, *o*-VA + INH → V) HOMO – 1 → LUMO (37%, *o*-VA + INH → INH + V)
	392	0.2386	HOMO → LUMO + 3 (74%, *o*-VA → V) HOMO – 1 → LUMO (10%, *o*-VA + INH → INH + V)
320	304	0.0706	HOMO – 3 → LUMO + 1 (25%, EtO → V) HOMO – 4 → LUMO + 1 (25%, INH + EtO + V=O → V) HOMO – 1 → LUMO + 4 (17%, *o*-VA + INH → *o*-VA + INH + V) HOMO – 2 → LUMO (11%, *o*-VA + INH → INH + V)
273	257	0.2297	HOMO – 4 → LUMO + 2 (31%, INH + EtO + V=O → V=O) HOMO – 1 → LUMO + 6 (28%, *o*-VA + INH → V + EtO) HOMO → LUMO + 7 (25%, *o*-VA → V=O)
234	231	0.121	HOMO – 7 → LUMO (69%, *o*-VA + INH → INH + V) HOMO – 3 → LUMO + 4 (11%, EtO → *o*-VA + INH + V)
	228	0.1047	HOMO – 2 → LUMO + 4 (49%, *o*-VA + INH → *o*-VA + INH + V) HOMO – 3 → LUMO + 4 (14%, EtO → *o*-VA + INH + V) HOMO → LUMO + 8 (11%, *o*-VA → *o*-VA)
	222	0.1851	HOMO – 7→ LUMO + 3 (28%, *o*-VA + INH → V) HOMO – 11 → LUMO (17%, *o*-VA + H_2O → INH + V) HOMO – 10 → LUMO + 1 (15%, *o*-VA + V=O → V) HOMO – 8 → LUMO + 2 (14%, *o*-VA + INH → V=O)

It can be seen from the proposed assignment that intraligand (IL) transitions within INHOVA are strongly coupled with ligand-to-metal charge transfer (CT) transitions. The experimental band observed at 424 nm is assigned to both IL and CT transitions. The band at 320 nm is found to be described by both IL and CT transitions with further contributions originated in transitions from the ethoxo and VO moieties to V. The experimental band at 273 nm exhibits mainly CT transitions from both INHOVA and ethoxo

to V and the VO group with some contribution of a transition from INHOVA to the ethoxo moiety. Finally, the band recorded at 234 nm is assigned mainly to IL and CT transitions. Comparison with free INHOVA electronic spectra (see Table 4 in ref. 25) shows that coordination to VO shifts absorption bands to higher wavelengths. HOMO and HOMO – 1 are essentially the same both in INHOVA and in (**1**): they are located in the ligand with no contribution from V or VO, see Figure 5. However, the LUMO presents contribution from *d* atomic orbitals of V ion and, moreover, LUMO + 2 in free INHOVA becomes LUMO + 4 in the complex, also exhibiting contributions from *d* atomic orbitals of V ion (Figure 5). The contribution of *d* atomic orbitals of V to unoccupied MO stabilizes both LUMO and LUMO + 4, thus leading to transitions with lower energies and, thus, higher wavelengths. With those arguments in mind, we notice that the bands at 222 and 304 nm in free INHOVA correspond to the calculated transitions found at 320 and 424 nm in the complex under study. The band at 336 nm in free INHOVA could be associated to a calculated transition at 500 nm in the complex, with almost negligible oscillator strength of 0.03 atomic units.

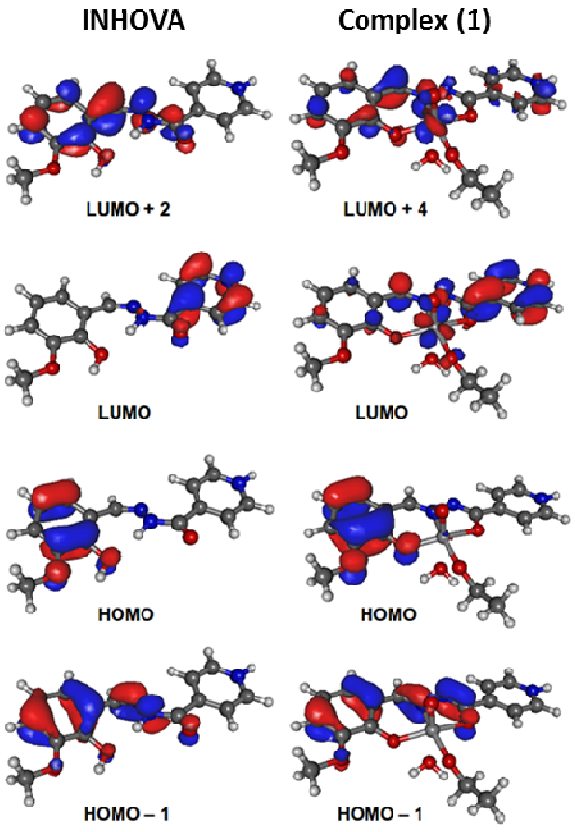

Figure 5. Comparison of frontier orbitals of INHOVA and the complex under study involved in some electronic transitions that describe their electronic spectra. Note the presence of *d* orbitals of the V(V) ion in both LUMO and LUMO + 4 in the complex.

3.5. Electrochemical characterization of INHOVA and Complex (1)

The redox behavior of the hydrazone ligand and the complex (**1**) are studied by cyclic voltammetry in DMSO and EtOH solutions. The compounds are stable in both solutions during the measurement time. However, in DMSO several adsorption processes modify the electrode surface leading to no reproducible voltammograms and erratic results. For this reason, only the results obtained for complex (**1**) in EtOH are considered and compared with those of the hydrazone ligand in the same experimental conditions. Cyclic voltammograms are obtained at several scan rates (v) and potential ranges to determine the nature of the individual processes.

Figure 6 shows a representative cyclic voltammogram, at v = 0.1V/s, of each compound between +1.4V and -2.2V vs Ag/Ag^+. As can be seen in the figure, the voltammogram of the ligand shows only one anodic current peak (A) at +0.69V. At a potential more positive than +1.0 V, decomposition current of the solvent occurs. When increasing scan rates (from 0.05 to 2V/s) are used to analyze the oxidation process, a positive shift of the anodic peak potential (Epa) is observed. On the return scan, at all scan rates investigated, no reduction current peak directly associated with this oxidation is observed. However, a small wave, which depends on the oxidation path, appears at -0.65V (data not shown). The electrochemical response is similar to the observed for the *o*-HVA precursor in DMSO [30]. It can be interpreted in terms of an oxidation charge transfer process followed by a fast chemical reaction [31]. Thus, according to the reported results, the anodic peak can be attributed to the oxidation of the -OH group of the o-HVA residue of the hydrazone ligand. After this oxidation path, a fast chemical reaction generates a new electrochemically active compound that is reduced, on the return scan, at the potential of the mentioned small wave [30]. This oxidation process (A) is absent in the cyclic voltammogram of the complex, where the OH group is deprotonated due to coordination to the metal center.

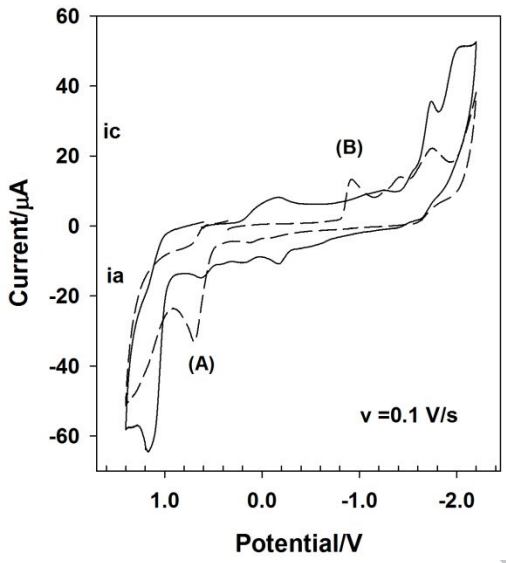

Figure 6. Comparative–ciclic voltammograms of complex(**1**) (—) and INHOVA (---) at v = 0.1 V s^{-1}. Solution: EtOH/$LiClO_4$.

On the other hand, the voltammetric reduction of the ligand gives rise to three cathodic processes in the potential range between -0.8V and -2.2V. Moreover, at all scan rates analyzed, these peaks do not display any reverse signal on the subsequent anodic scan and the cathodic peak potentials (Epc) are shifted toward more negative values as the scan rate increases (data not shown). The first cathodic peak (B) in the voltammogram could be ascribed to the reduction of the -CH=N-NH- moiety [32]. This process probably leads to the cleavage of the single N-N bond with the consequent formation of new species, which are reduced at more negative potentials.

The electrochemical behavior of complex (**1**) is studied in the same conditions as those discussed for the ligand. Fig. 6, illustrates a typical cyclic voltammogram of the vanadium complex where three main irreversible current peaks are evident. From the available electrochemical data it can be stated that, at the initial potential of +0.6V the electroactive species is the V(IV) complex. The small waves in the potential range between +0.2V and -0.4V are due to adsorption/desorption processes on the electrode surface and are not discussed here.

As can be seen from the Figure, complex (**1**) is reduced at more negative potentials than the free ligand. On the forward cathodic scan two well defined peaks at -1.75V and -2.0V are observed, without anodic counterpart at all scan rates analyzed. As v increases, these peaks shift toward more negative potential and no evidence of chemical reactions either

preceding or following the electrode process are observed (data not shown). Thus, it is possible to infer that both reductions are irreversible. For comparison with the behavior of the free ligand the first one could be ascribed to a ligand-centered process that probably involves the reduction of the –CH=N-N=CO coordinated moiety. Moreover, the metallic center is reduced to V(III) at -2.0V, whereas the anodic peak observed at +1.15V on the return scan can be assigned to the oxidation of the metal center to V(V). This last process is also evident when the potential sweep is first run in positive direction, showing that is independent of the reduction processes that occur at negative potentials.

3.6. Cytotoxicity assays

Both INHOVA and its oxidovanadium(V) complex showed cytotoxic activity in K562 cells, in a concentration-dependent manner. The activity presented by (**1**) is slightly higher than that of its ligand: concentrations required to inhibit 50% of cellular growth, the IC_{50} values, are 28.80 ± 3.48 μM and 36.46 ± 4.13 μM, respectively. These values are the mean of four independent determinations. The reference metallodrugs cisplatin and carboplatin show IC_{50} values of, respectively, 1.1 μM and 10.0 μM in the same experimental conditions [33]. However, due to the toxic side effects associated to platinum and to the emergence of resistant tumors, the search for new metal-based antitumor agents constitutes a field in continuous growth. Concerning V compounds, Meshkini and Yazdanparast described the chemosensitization of human leukemia K562 cells to taxol by a vanadyl salen complex. Besides, the complex itself was able to inhibit the proliferation of K562 cells. [34]. Lampronti and co-workers [35] studied the effects of a series of vanadium complexes on the growth of K562 cells. Authors conclude that the complexes in which vanadium presents a +5 oxidation state, along with their discrete anionic units, appear critical for the respective effects on those cells. In a recent review, Novotny and Kombian state that, in spite of the work published on the subject, our knowledge on the potential use of vanadium complexes as anticancer agents is to date lacking. In this sense, many preclinical, clinical and epidemiological studies are needed [36]. With the purpose of contribute to a better understanding of the antiproliferative activity of oxidovanadium(V) compounds and their related putative use in cancer therapy, and in view of the results presented here, we suggest both INHOVA and complex (**1**) as good candidates for further pharmacological investigations.

4. Conclusions

A novel and stable ester-like complex, [VO(INHOVA) EtO(OH_2)]Cl·H_2O, was obtained from the interaction of oxovanadium chloride with the INHOVA hydrazone, the condensation product of isoniazid and *o*-vanillin.

The crystal structure of the chloride salt of the cationic complex shows that INHOVA acts as a tridentate (O,N,O´) ligand and that it is present as a monoanion, due to the protonation of the pyridinic nitrogen.

The distorted octahedral environment of the vanadium centre is completed with the oxo moiety, a disordered ethoxide group and a water molecule. The complex cations aggregate into a dimer by means of intermolecular H-bonds. The interaction with chlorides and crystallization water molecules stabilizes the bilayer overall arrangement.

A detailed spectroscopic analysis has been performed. The FTIR spectrum of the solid shows the effect of coordination on the ligand vibrational modes and the appearance of vibrations involving the metal center were observed. Computational calculations based on DFT, including geometry optimization, were performed and employed to assist in the spectra interpretation. They predict a strong coupling among different modes and help in the assignment of the bands.

Characterization in solution was carried out and data were also analyzed in comparison with the free ligand behavior.

The electronic spectra show the changes in electronic distribution upon the complexation. Shifts in the intra-ligand transitions and the occurrence of charge transfer bands can be observed. Calculations were relevant in the spectra interpretation and denote that each absorption band can be described for more than one single-electron transition.

As expected, cyclic voltametric measurements show that deprotonation and coordination to the metal center modify the redox behavior of INHOVA. Additionally, signals related to vanadium oxidation-reduction process appear in the cyclic voltammogram of the complex.

Citotoxicity assays against the *chronic myelogenous leukemia* K562 cell line show that both (**1**) and INHOVA can be considered candidates for further investigations.

Appendix A. Supplementary data

CCDC 1551305 contains the supplementary crystallographic data for complex (**1**) (formula: C16 H19 N3 O6 V1 1+,H2 O1,Cl1 1-). These data can be obtained free of charge via http://www.ccdc.cam.ac.uk/conts/retrieving.html, or from the Cambridge

Crystallographic Data Centre, 12 Union Road, Cambridge CB2 1EZ, UK; fax: (+44) 1223-336-033; or e-mail: deposit@ccdc.cam.ac.uk.

A complete list of frequencies and respective assignments of IR spectra of INHOVA and complex (**1**) are provided as Supplementary Material (Table S1).

Acknowledgements

This work was supported by CONICET (CCT-La Plata) and UNLP Argentina. R.P.D., B.S.P.C. and A.C.G.B. are members of the Research Career of CONICET. NAR wishes to thank CNPq (Conselho Nacional de Desenvolvimento Científico e Tecnológico, Brazil) and FAPERJ (Fundação Carlos Chagas Filho de Amparo à Pesquisa do Estado do Rio de Janeiro, Brazil) for the fellowships awarded. JALCR wishes to thank CNPq (Conselho Nacional de Desenvolvimento Científico e Tecnológico, Brazil) for the fellowship awarded. The authors acknowledge Universidad Nacional de Catamarca, Argentina, for computing time. The authors also thanks to LDRX/UFF (FAPERJ) for the x-ray data.

References

[1] B. Villemagne, C. Crauste, M. Flipo, A.R. Baulard, B. Déprez, N. Willand, Eur. J. Med. Chem. 51 (2012) 1-16 (and references therein).
[2] A. Zubrys, C.O. Siebenmann, Can. J. Chem. 33 (1955) 11-14.
[3] R. Maccari, R. Ottanà, M.G. Vigorita, Bioorg. Med. Chem. Lett. 15 (2005) 2509-2513.
[4] M.A. Bhat, M.A. Al-Omar, Med. Chem. Res. 22 (2013) 4522–4528.
[5] S.W. Chen, H.D. Yin, D.Q. Wang, X. Kong, X.F. Chen, Acta Cryst. E62 (2006) o2043–o2044.
[6] D.S. Yang, J Chem Crystallogr 37 (5) (2007) 343-348.
[7] H. Ozay, M. Yildiz, H. Unver, A. Kiraz, Crystallogr. Rep. 58 (1) (2013) 106–110.
[8] A.C. González-Baró, R. Pis-Diez, B.S. Parajón-Costa, N.A. Rey, J. Mol. Struct. 1007 (2012) 95–101.
[9] L. Narayana Suravapu, Y. Kyo Seo, S.O.O. Baek, V.R. Ammireddy, E. J. Chem. 9 (2012) 1288-1304.
[10] M.R. Maurya, S. Agarwal, M. Abid, A. Azam, C. Bader, M. Ebel, D. Rehder, Dalton Trans. (2006) 937-947.
[11] P. Krishnamoorthy, P. Sathyadevi, A.H. Cowley, R.R. Butorac, N. Dharmaraj, Eur. J. Med. Chem. 4(2011) 3376-3387.
[12] M.L. Ferreir, R.S.B. Gonçalves, L.N.F. Cardoso, C.R. Kaiser, A.L.P. Candéa, M.G.M.O. Henriques, M.C.S. Lourenço, F.A.F.M. Bezerra, M.V.N. de Souza, Sci. World. J. 10 (2010) 1347–1355.
[13] R. Maccar, R. Ottana, B. Bottari, E. Rotondob, M.G. Vigorita, Bioorg. Med. Chem. Lett. 14 (2004) 5731–5733.

[14] M. Hong, H. Geng, M. Niu, F. Wang, D. Li, J. Liu, H. Yin, Eur. J. Med. Chem. 86 (2014) 550-561.
[15] E. Kioseoglou, S. Petanidis, C. Gabriel, A. Salifoglou, Coord. Chem. Ver. 301-302 (2015) 87–105.
[16] S. Matsugo, K. Kanamori, H. Sugiyama, H. Misu, T. Takamura, J. Inorg. Biochem. 147 (2015) 93–98.
[17] D. Rehder, Metallomics 7 (2015) 730-742.
[18] Q. Guo, L. Li, J.J. Dong, H. Liu, T. Xu, J. Li, Spectrochim. Acta A 106 (2013) 155–162.
[19] A.C. González Baró; O.E. Piro, B.S. Parajón Costa, E.E. Castellano, E.J. Baran, Monatsh. Chem. 129 (1998) 31-39.
[20] B.S. Parajón Costa, A.C. González Baró, E.J. Baran, J. Coord. Chem. 49 (1999) 17-31.
[21] M.R. Maurya, S. Khurana, C. Schulzke, D. Reahder, Eur. J. Inorg. Chem. 3 (2001) 779-788.
[22] M.R. Maurya, S. Agarwal, C. Bader, M. Ebel, D. Rehder, Dalton Trans. (2005) 537-544.
[23] H.H. Monfared, R. Bikas, P. Mayer, Inorg. Chim. Acta 363 (2010) 2574-2583.
[24] H.K. Wong, K. M. Lo, S. Weng Ng Acta Cryst. E. 67 (2011) m799-m799.
[25] S. Grimme, J. Comp. Chem. 27 (2006) 1787-1799.
[26] C. Adamo, V. Barone J. Chem. Phys. 110 (1999) 6158-6170.
[27] J. Tomasi, B. Mennucci, E. Cancès, J. Mol. Struct. (Theochem) 464 (1999) 211-226.
[28] Gaussian 09, Revision B.01, M.J. Frisch, G.W. Trucks, H.B. Schlegel, G.E. Scuseria, M.A. Robb, J.R. Cheeseman, G. Scalmani, V. Barone, B. Mennucci, G.A. Petersson, H. Nakatsuji, M. Caricato, X. Li, H.P. Hratchian, A.F. Izmaylov, J. Bloino, G. Zheng, J.L. Sonnenberg, M. Hada, M. Ehara, K. Toyota, R. Fukuda, J. Hasegawa, M. Ishida, T. Nakajima, Y. Honda, O. Kitao, H. Nakai, T. Vreven, J.A. Montgomery Jr., J.E. Peralta, F. Ogliaro, M. Bearpark, J.J. Heyd, E. Brothers, K.N. Kudin, V.N. Staroverov, T. Keith, R. Kobayashi, J. Normand, K. Raghavachari, A. Rendell, J.C. Burant, S.S. Iyengar, J. Tomasi, M. Cossi, N. Rega, J.M. Millam, M. Klene, J.E. Knox, J.B. Cross, V. Bakken, C. Adamo, J. Jaramillo, R. Gomperts, R.E. Stratmann, O. Yazyev, A.J. Austin, R. Cammi, C. Pomelli, J.W. Ochterski, R.L. Martin, K. Morokuma, V.G. Zakrzewski, G.A. Voth, P. Salvador, J.J. Dannenberg, S. Dapprich, A.D. Daniels, O. Farkas, J.B. Foresman, J.V. Ortiz, J. Cioslowski, D.J. Fox, Gaussian Inc. Wallingford CT (2010).
[29] D. Cook, Can. J. Chem. 39 (1961) 2009-2014.
[30] A.C. Gonzalez Baro, R. Pis-Diez, C.A. Franca, M.H. Torre, B.S. Parajon Costa Polyhedron 29 (2010) 959–968.
[31] A.J. Bard, L.R. Faulkner in: Electrochemical Methods: Fundamentals and Applications, second ed., J. Wiley & Sons, New York, 2001.
[32] V.D. Parker, in: Organic Electrochemistry, M.M. Baizer (Ed.) Marcel Dekker, New York, 1973.
[33] J.C. Almeida, I.M. Marzano, M. Pivatto, N.P. Lopes, A.M.C. Ferreira, F.R. Pavan, I.C. Silva, E.C. Pereira-Maia, G. Poelhsitz , W. Guerra, Inorg. Chim. Acta 446 (2016) 87–92.
[34] A. Meshkini, R. Yazdanparast Exp. Mol. Pathol. 89 (2010) 334-342.

[35] I. Lampronti, N. Bianchi, M. Borgatti, E. Fabbri, L. Vizziello, M.T. Khan, A. Ather, D. Brezena, M.M. Tahir, R. Gambari, Oncol. Rep. 14 (2005) 9-15.
[36] L. Novotny, S.B. Kombian J. Can. Res. Updates 3 (2014) 97-102.

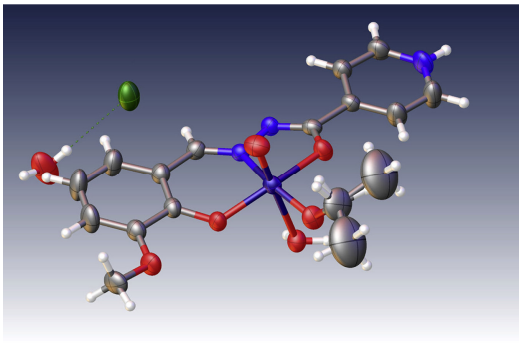

Graphycal Abstract

A oxidovanadium(V) complex with a hydrazone ligand of isoniazid and *o*-vanillin was obtained. Its crystal structure was determined. It was fully characterized by means of spectroscopic and electrochemical methods. The assignments were accomplished with the help of theoretical calculations based on DFT methods. It showed cytotoxic activity in K562 cells.